The 9TH European Review Meeting on Severe Accident Research (ERMSAR2019) **Log Number: 039**
Clarion Congress Hotel, Prague, Czech Republic, March 18-20, 2019

Main outcomes from the IVR code benchmark performed in the IVMR project

L. Carénini[1], F. Fichot[1], N. Bakouta[2], A. Filippov[3], R. Le Tellier[4], L. Viot[4], I. Melnikov[5], P. Pandazis[6]

[1]: IRSN, BP3 – 13115 St Paul lez Durance - FRANCE
[2]: EDF, EDF Lab, Paris-Saclay, 7 boulevard Gaspard Monge, 91120 Palaiseau, FRANCE
[3]: IBRAE, 52 B. Tulskaya St. Moscow, RUSSIA
[4]: CEA, DEN, DTN/SMTA/LMAG, Cadarache – 13108 Saint Paul-lez-Durance - FRANCE
[5]: NRC-KI, 1, Akademika Kurchatova pl., Moscow, 123182, RUSSIA
[6]: GRS, Boltzmannstraße 14, 85748, Garching, GERMANY

laure.carenini@irsn.fr, florian.fichot@irsn.fr, nikolai.bakouta@edf.fr, phil@ibrae.ac.ru, romain.le-tellier@cea.fr, louis.viot@cea.fr, Melnikov_IA@nrcki.ru, Peter.Pandazis@grs.de

Abstract

In-Vessel Retention (IVR) of corium is one of the possible strategies for Severe Accident (SA) mitigation. Its main advantage lies in the fact that, by maintaining the corium within the vessel, the integrity of the last containment barrier against corium aggression is preserved. One of the issues for the demonstration of the success of this strategy is the evaluation of the behaviour of the corium relocated in the lower head and how it stabilizes and affects the integrity of the vessel wall. The first modelling was developed in the nineties and assessed the heat transfers in a stratified corium pool with a top metal layer made of steel and Zirconium only. About 10 years later, the results of the MASCA program highlighted the possibility of having more complex stratified configurations, including a dense metal layer. Addressing thermochemical effects on the stratification makes the modelling of the corium pool in the lower head more difficult and, in addition, knowledge of the associated kinetics is still limited. As a consequence, available SA codes, either integral or dedicated to the lower head, can differ significantly in their models, which leads to discrepancies in the results when evaluating the IVR strategy.

In order to identify the main modelling issues and to assess the capabilities of the codes, a benchmark exercise for code validation was made in the scope of the European H2020 project IVMR (In-Vessel Melt Retention). It is based on the definition of different IVR configurations at reactor scale with an increase in the complexity of the phenomena involved: starting from a steady-state stratified pool with metal on the top, up to consideration of corium phase separation at thermochemical equilibrium and progressive ablation of metallic structures and vessel wall. In this paper, the main results and outcomes obtained are presented and discussed. Six organisations took part in this benchmark (CEA, EDF, GRS, IBRAE, IRSN, NRC-KI) and 6 different codes were used (ASTEC, ATHLET-CD, MAAP_EDF, PROCOR, HEFEST_URAN and HEFEST – stand-alone version of the corresponding module of the SOCRAT code). Finally, sensitivity studies are performed and allow obtaining a more consolidated range of results.

Thanks to this benchmark exercise and to the approach followed with a progressive increase of complexity, the capabilities of codes to evaluate the heat flux profile applied to the vessel wall in steady-state are demonstrated. Then, the larger differences between code results obtained in transient situations have been identified and associated modelling assumptions discussed.

Keywords: IVR strategy, SA codes benchmark, stratified corium pool evolution

1. Introduction

During a Severe Accident (SA) in Light Water Reactor (LWR), the lack of fuel cooling in the reactor vessel leads to core heat up and then melting of materials. The melt flows down to the lower plenum of the vessel. Consequently, the main part of the power generated by the fuel is not produced in the core zone anymore but at the bottom of the reactor pressure vessel (RPV). In such situation, a strategy of external cooling of the vessel wall (ERVC) to maintain the integrity of the vessel and to stabilize the corium inside the RPV may be used. This would reduce significantly the threats to the last barrier (the containment) and therefore reduce the risk of large release of low-volatile radioactive products to the environment. This In-Vessel Retention (IVR) strategy was introduced about 20 years ago (Henry and Fauske, 1993; Tuomisto and Theofanous, 1994). It was first applied to two designs of reactors: the AP600 (Theofanous et al., 1997), later replaced by the AP1000 design (Esmaili et al., 1997), and the VVER-440 (Kymälainen et al., 1997). Today, new reactor designs have been developed including this IVR strategy and first units become progressively operational: the Korean APR-1400 design (Knudson et al., 2004; Rempe et al., 2004; Whang et al., 2017) and the Chinese HPR-1000 design (Xing, 2017). At the same time, the possibility to apply IVR strategy as back-fitting measure to existing GEN II reactors is currently under consideration. In particular, the VVER1000 design attracts a lot of interest (Zdarek et al. 2013; Gencheva et al. 2016; Duspiva 2017).

Since the first evaluations performed in the nineties and the associated modelling developments, progresses in the understanding of the thermochemistry of the corium in the lower head when mixed with molten steel were made, mainly thanks to the results of the OECD MASCA 2 program (Tsurikov, 2007). Indeed, it was found that the chemical interactions in the melt pool have a direct impact on its stratification and need to be considered in the evaluations of IVR strategy. It appears then necessary to be able to describe the transient coupled thermal-hydraulics and chemical interactions scenario that occurs in the melt pool to estimate the thermal load on the vessel wall. That makes the situation much more complicated for code modelling compared to the previous standard configuration with the oxide pool being always below a top metal layer composed only with steel and Zirconium. In addition, the validation of such complex models needs further experimental efforts with prototypic materials.

As a consequence, available SA codes, either integral or dedicated to the lower head, can differ significantly in their models, which leads to discrepancies in the results when evaluating the IVR strategy. This issue was highlighted in the scope of the European H2020 project IVMR (In-Vessel Melt Retention), which aims revisiting the SA strategy of IVR, in particular for reactor of ‘‘high-power”, i.e. 1000 MWe or more (Fichot et al. 2018). In order to identify the main modelling issues and to assess the capabilities of the codes, a benchmark exercise was made with the codes’ developers involved in the project: CEA with PROCOR, EDF with a proprietary version of MAAP (derivative of EPRI’s MAAP5 code, referred to as MAAP_EDF in this paper), GRS with AIDA module of the ATHLET-CD code, IBRAE with HEFEST_URAN, IRSN with ASTEC and NRC-KI with HEFEST – stand-alone version of corresponding module of the SOCRAT code.

The description of this benchmark as well as the main results and outcomes are presented in this paper.

2. Objectives and scope of the benchmark exercise

This benchmark exercise involves several calculations defined with a progressive increase of complexity. From a standard configuration of corium layering in steady state with the metal layer on the top, it is proposed to investigate a transient situation considering a progressive increase of the mass of molten steel incorporated in the corium pool. The idea is to follow the variation of the heat fluxes applied to the vessel wall with time and compare the vessel wall ablation once reaching a steady state. Then, the effects of thermochemistry in the corium pool are investigated based on the same transient configuration.

To define the first step, the benchmark case used in the scope of AP600 and AP1000 designs development (Rempe et al., 1997; Esmaili and Khatib-Rahbar, 2004) was considered. Thus, the vessel geometry and the initial characteristics of the corium pool are specified (composition, residual power) and two tests are proposed depending on the assumption considered for the boundary condition on the top surface of the pool: adiabatic (test n°1) or radiative heat transfers towards surrounding structures considered at 950K (test n°2). Tests specifications are summarized in Figure 1. For such simple configurations, thermochemistry in the corium pool is neglected and an analytical evaluation of heat fluxes at the boundaries of each layer and of the layer temperatures is possible (cf. Appendix) and is then used for comparison with codes results. The vessel wall is considered only as a temperature boundary condition equal to the liquidus temperature of the stainless steel.

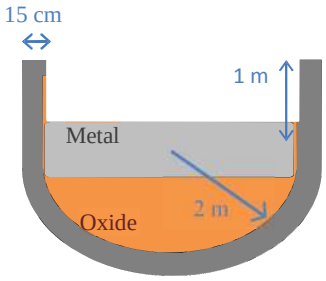

Parameter	Value
Oxide pool	
Height of the oxide pool	1.5 m
Composition	0.8 UO_2 - 0.2 ZrO_2 (mass fraction)
Residual power	14 MW
Metallic pool	
Height of the metallic pool	0.9 m
Composition	0.9 stainless steel – 0.1 Zr (mass fraction)

Figure 1 Geometry of the lower head and corium configuration considered for the benchmark tests n°1 and 2

As a second step, in order to study transient effect, an additional test is proposed, in which the overall corium composition and decay heat at relocation in the lower head are imposed (as in previous tests), but the mass of molten steel incorporated increases progressively according to a given kinetics to simulate the progressive melting of the metallic structures in the reactor vessel. Besides, the molten steel addition due to the vessel wall melting is also simulated, up to the steady state. In this case, the efficiency of the external vessel cooling is assumed and simulated using an imposed boundary condition (heat flux coefficient and water temperature). Firstly, the thermo-chemical equilibrium in the U-O-Zr-Fe quaternary system is not simulated (test n°3) as it is the case in steady state configurations described before.
In a third step, it is proposed to activate the evaluation of the thermochemistry in the codes (when available) to identify the impact on the corium stratification (test n°4). It should be noted that in this last case the mass of non-oxidized Zirconium is not assumed to be mixed with the molten steel initially but with the oxide pool and the metal phase separation is expected to be evaluated by the code.

Table 1 Corium characteristics considered for the benchmark tests n°3 and 4

Parameter	Test n°3	Test n°4
Oxide pool		
Height of the oxide pool	1.5 m	-
Composition	0.8 UO_2 - 0.2 ZrO_2 (mass fraction)	UO2 mass 68t ZrO2 mass 17t Zr mass 7.5t
Residual power	14 MW	
Metallic pool		
Initial mass of Zr	7.5t	-
Initial mass of steel	30t	
Top relocation of molten steel from 9000s to 14000s	6kg/s	

Finally, sensitivity calculations were performed based on the last transient configuration introduced above, which is the more complete and involved all the relevant phenomena. The main parameters identified as leading to the main differences in the steady-state configurations studied in the first step of the benchmark exercise were considered, in the range between lower and upper values implemented by default in the different codes used.

3. Main features of codes

The main modelling choices made in the six codes involved in this benchmark exercises are summarized in Table 2. The differences in terms of meshing for the vessel wall, the corium pool and the oxide crust are mentioned. In addition, the availability of a model to deal with thermochemical aspects in the corium pool is mentioned. The detail of these models will be discussed further in part 4.3, dealing with results obtained for test n°4.
More information about code capabilities may be found in associated publications Carénini and Fichot (2016) for ASTEC, Pandazis and Weber (2018) for ATHLET-CD, , Filippov et al. (2010) for HEFEST_SOCRAT, Filippov et al. (2014) for HEFEST_URAN, Bakouta et al. (2017) for MAAP_EDF and Le Tellier et al. (2015) for PROCOR.

Table 2 Main features of lower head modelling in codes

	ASTEC	ATHLET-CD	HEFEST-SOCRAT[1]	HEFEST-URAN[1]	MAAP_EDF	PROCOR
Vessel wall	2D meshing	2D meshing	2D meshing	2D meshing	2D meshing	1D axial meshing
Corium pool	Up to 3 layers	2 layers	2D meshing	2D meshing	Up to 3 layers	Up to 4[2] layers
Oxide crust	Thermal resistance	Explicitly modeled in 2D with the vessel, not considered between oxide and metal layers	Explicitly modeled	Explicitly modeled	Explicitly modeled	Thermal resistance and physical barrier for chemical interaction
Thermo-chemical equilibrium in U-O-Zr-Fe system	Yes	No	Yes	Yes	Yes	Yes

4. Results and outcomes

4.1 Steady-state configurations

For steady-state configurations, two different boundary conditions have been simulated for the top of the metal layer, modelling or not the radiative heat transfers (respectively referred to as test n°2 and n°1). The results obtained for the average heat fluxes at the boundaries of the corium pool and between layers are summarized in Figure 2. A good agreement between the evaluations may be observed with dispersion below 10% in the adiabatic case and up to 17% for the heat flux from the metal layer to the vessel wall in the test n°2, directly associated to the variation in the radiative heat flux evaluated at the top of the metal layer (variation around 50%).

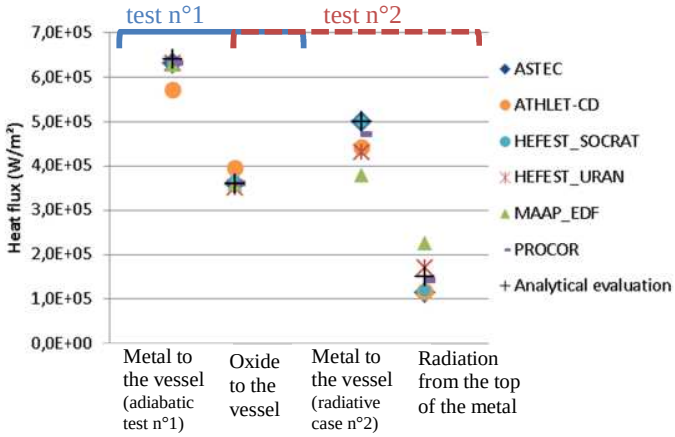

Figure 2 Average heat fluxes evaluated for the benchmark tests n°1 and 2

[1] The difference between the HEFEST code versions implemented in the HEFEST_URAN package and in the SOCRAT code is due to the presence of some additional models in HEFEST_URAN: enclosure radiation, in-vessel melt relocation from the core barrel, FAS-model (detailed consideration of side-wall heat flux), models of melt-water interaction, shrinkage and some other used for in-vessel and ex-vessel melt simulations. But the solver and kernel models of melt-structure interaction are practically the same in the both versions, and the listed additional models were not activated in the benchmark calculations performed with HEFEST_URAN. However, for this benchmark, default heat transfer model of HEFEST module (based on effective thermal conductivity and described in the paper (Filippov et al., 2014)) was not used in HEFEST_SOCRAT simulations and a model with boundary-controlled heat transfer coefficient (HTC) was chosen. The correlations for HTC correspond to analytical solution.

[2] When stratification inversion occurs, an additional metal layer below the oxidic crust and above the oxidic pool appears based on the assumption that the oxidic crust is stable (see §4.3).

Even if such variations (below 20%) for the heat flux applied to the vessel wall may be considered as acceptable regarding the IVR issue, these simple configurations were studied further in order to identify the main reason for the variation of the heat flux evaluated by the different codes.
The first difference is associated to the correlation chosen for the heat transfers in the oxide pool, which determines the power split between the lateral surface with the vessel and the top surface. It is evaluated to 0.44 in ATHLET-CD code which uses Asfia-Dhir correlation (1996) in the presented simulation for the heat transfers towards the vessel[3] compared to 0.52±0.01 in other codes based on COPO/BALI correlations (Bonnet and Seiler, 1999). This difference mainly explains the discrepancy in the heat flux profiles evaluation with ATHLET-CD and the other codes (cf. Figure 3, test n°1), especially the underestimation of the heat flux at the top layer location since the power transmitted from the oxide pool to the metal layer is reduced of about 8%. It should be highlighted that Asfia-Dhir correlation is valid for Rayleigh numbers $2.10^{10} < Ra_i < 10^{14}$, whereas COPO/BALI correlation is applicable to higher values $10^{13} < Ra_i < 10^{17}$ and thus more adapted to the current simulations ($Ra_i \sim 3.10^{15}$, cf. Appendix).

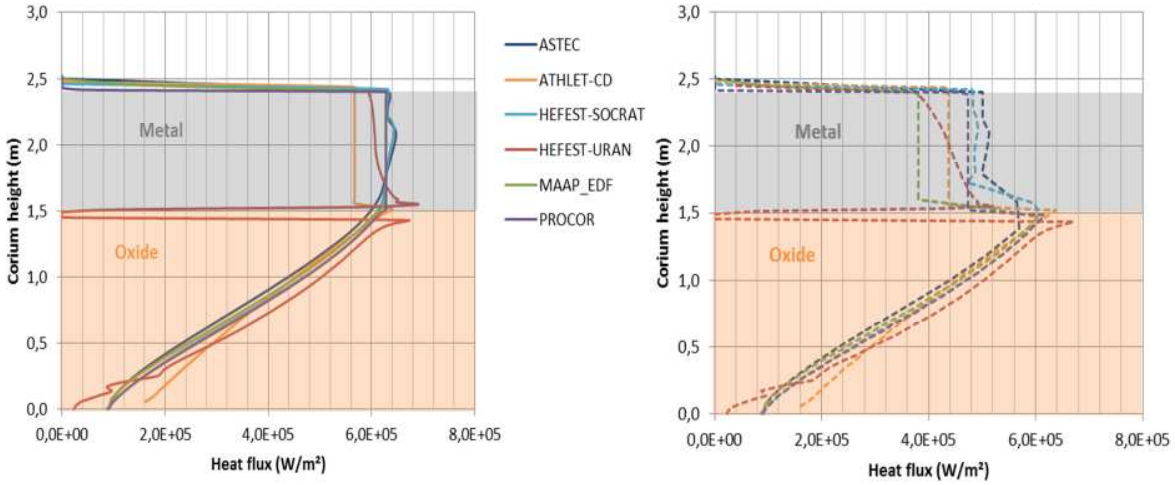

Figure 3 Heat flux profiles evaluated at steady state for the benchmark test n°1 (left) and test n°2 (right)

Regarding the heat flux profile along the vessel wall, which determines the maximum value of heat flux, it is observed that all codes have similar correlations for the hemispheric part of the wall, with a comparable value evaluated for the maximum heat flux at the top of the oxide pool. In HEFEST-URAN simulation, at the location of the oxide crust, the heat flux to the vessel wall is drastically reduced due to the thin insulating layer introduced between the oxide and metal layers. Heat transfer from oxide to metallic layer is modelled here as an equivalent heat source in the metallic layer that is described in Filippov et al. (2014). High nonuniformity of material properties in this point leads to local peaks of heat flux a both sides of the phase boundary. This peak eliminates in realistic case when metal and oxide layers contact with the vessel.
In Figure 4, the temperatures obtained for the layers are synthetized. It appears that significant differences may happen due to differences in the material properties considered. It is recalled that it was recommended to use the default value of material properties available in each code. The range of variation is summarized in Table 3.

[3] For the heat transfers towards the top surface of the oxide pool, the correlation of Kelkar (Kelkar et al., 1993) is used in ATHLET-CD.

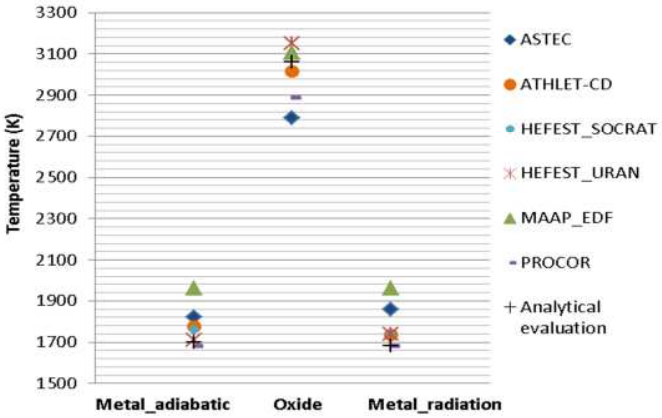

Figure 4 Layers temperatures evaluated at steady state for the benchmark tests n°1 and 2

Table 3 Range of variation of layers properties considering all the different codes[4]

	Parameter	Value	Variation
Oxide pool	Density	7711 - 8300 kg/m^3	±4%
	Thermal conductivity	**2.3 - 7.07 W/m/K**	**±51%**
	Dynamic viscosity	4.57 - 5.27x10^{-3} m²/s	±7%
	Specific heat capacity	520 - 604 J/kg/K	±7%
	Thermal expansion coefficient	**2.61x10^{-5} - 1. 05x10^{-4} K^{-1}**	**±60%**
	Melting temperature	2600 - 2950 K	±6%
Metallic pool	Density	6763 - 7156 kg/m^3	±3%
	Thermal conductivity	19.65 - 38.4 W/m/K	±32%
	Dynamic viscosity	**4.07x10^{-3} – 2.24x10^{-2} Pa.s**	**±69%**
	Specific heat capacity	538 - 789.5 J/kg/K	±19%
	Thermal expansion coefficient	**2.9x10^{-5} - 1.17x10^{-4} K^{-1}**	**±60%**
	Melting temperature	1600 - 1778 K	±5%
	Emissivity	0.2 - 0.4	±33%

Since the melting temperature of the oxide (resp. the metal) considered in the different codes varied in the range 2600K-2950K (resp. 1600K-1723K), it is better to compare the results in terms of layer superheat above its melting temperature as presented in Figure 5 (resp. Figure 6).

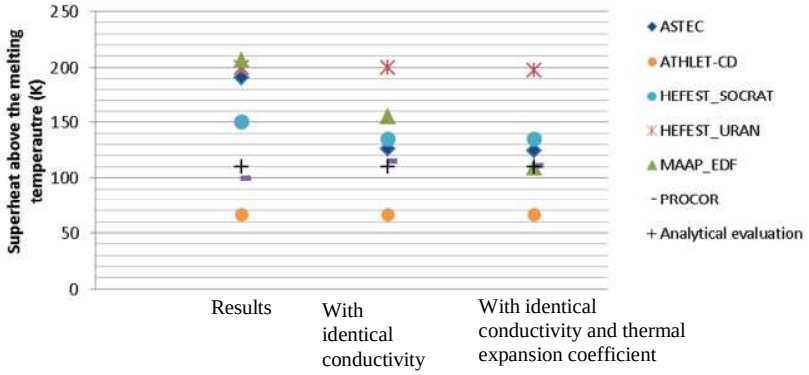

Figure 5 Oxide superheat and impact of dispersion in material properties (analytical evaluation being considered here as reference)

A significant spread of the results is observed for the oxide layer temperature. This can be related to the discrepancy in the value of the oxide conductivity and in the thermal expansion coefficient as illustrated in the graph with the

[4] Values evaluated when steady state is reached, i.e. at the corresponding temperature.

reduction of the dispersion when variation due to the value of the conductivity and then conductivity plus thermal expansion coefficient are considered. Indeed, the conductivity of the oxide layer has a significant dispersion (±51%) and considering COPO/BALI correlation, the conductivity of the oxide impacts the temperature super-heat at the power -0.5 (cf. appendix A). The dispersion of the thermal expansion coefficient is also significant (±60%) even if its contribution is reduced (power -0.25). For ATHLET-CD results, it should be noted that the material properties were taken equal to the one considered in the analytical calculation[5]. The discrepancies observed are not only due to the differences in correlations used for the heat transfers in the oxide pool mentioned before (in this case an overestimation of the oxide temperature would have been expected), but mainly to the fact that the oxide crust between the oxide pool and the metal layer is not simulated. With such assumption, the oxide behaviour is dependent on the characteristics of the metal layer, which is not the case in the evaluations performed with the other codes. In the analytical evaluation (cf. appendix A), the assumption of a crust between the oxide and the metal layer is also made, since such a crust is expected in the reactor case due to the temperature difference between the oxide and the metal. For HEFEST-URAN results, the reason for having a higher oxide temperature compared to the other codes is in insulating properties of solid crust formed in the cooled boundary. The temperature is sensitive to the solid layer heat resistance in these specific configurations where massive vessel wall is no modelled.
Regarding the metal layer temperature dispersion, the influence of the material properties with in particular, the viscosity and the thermal expansion coefficient may be highlighted (cf. Figure 6). The dispersion in the heat conductivity appears more limited compared to the one of the oxide layer. It is worth noting that the dispersion of the Prandtl number of the metal layer among the different simulations is significant: 0.08-0.8.
In addition to these effects, the correlation of heat transfers from the metal layer to the vessel wall may also play a role. All the codes use the Chawla and Chan correlation (1982) or equivalently the Churchill and Chu one, (1975) except ATHLET-CD in which the COPO/BALI correlations are used in the metal layer. In addition, the implementation of this correlation in ASTEC is done using the radius as characteristic length for the layer instead of its thickness as done in other codes and in the analytical evaluation presented in appendix. This choice was made to avoid non-physical results when the layer height tends to 0, leading to evaluate an infinite heat flux. This leads to multiply in this case the metal super-heat by a factor 1.25, as shown in Figure 6. Here again, the discrepancy in the evaluation from ATHLET-CD has to be associated to the fact that the thermal resistance from the oxide crust is neglected between the oxide and the metal, increasing the metal temperature.

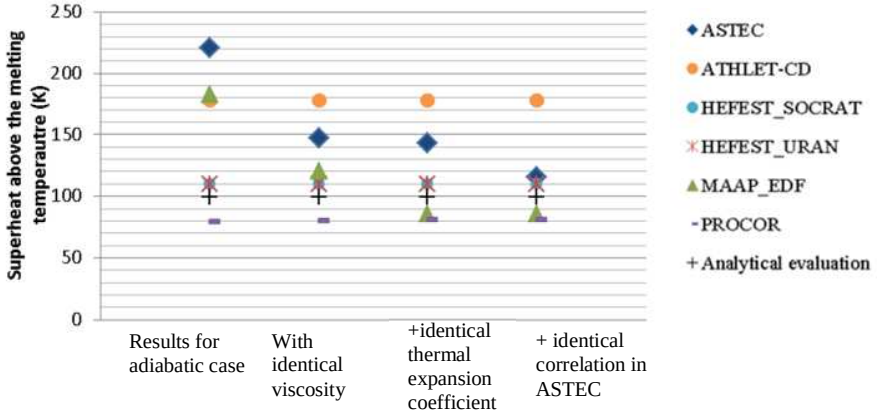

Figure 6 Metal super-heat in case n°1 and impact of dispersion *in material* properties (analytical case being considered as the reference here) and characteristics length

In case n°2, with top radiative condition, the dispersion of the metal layer temperature (cf. Figure 7 (a)) has also to be related with the dispersion in the emissivity considered for the radiative heat transfers (in the range 0.21-0.4 in those simulations). In this case, the relative influence of the material properties and of the correlations is more difficult to identify. Looking at the power split in the metal layer between radiation and convection towards the vessel wall (cf. Figure 7 (b)), a significantly higher value for the MAAP_EDF simulation is observed. This may be first related to the effect of the metal viscosity and thermal expansion coefficient, which impacts directly the temperature of the metal layer, as identified before (cf. Figure 6). Then, in this case, the melting temperature of the

[5] For properties defined in Table 4. For other properties, in particular dealing with the oxide crust formation, default values of ATHLET-CD codes are used.

layer is higher (1778K) compared to the analytical case (1600K) and it also plays a role in the increase of the power dissipated by radiative heat transfers. In comparison, for ASTEC simulation, the reduced power fraction dissipated by radiation considering the high super-heat of the layer should be linked to the emissivity of the metal layer which is considered equal to 0.21 in this simulation against 0.38 in MAAP_EDF case and in the analytical case. Those appear to be the main reasons for the lower value evaluated for the heat flux applied to the vessel wall in this case n°2 for the MAAP_EDF simulation (cf. Figure 3).

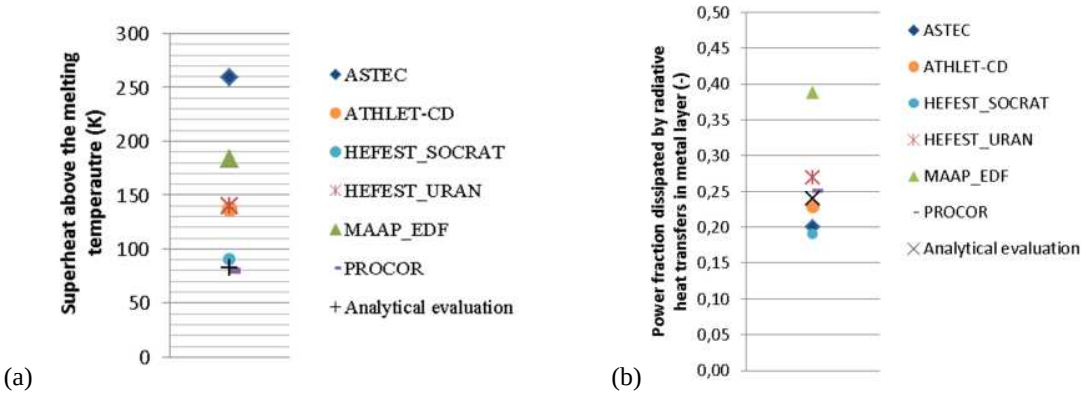

Figure 7 Metal superheat (a) and power fraction dissipated by radiation in the metal (b) in case n°2

To conclude this first part of the benchmark exercise, it was shown that, despite the simplicity of the configurations studied, a lot of interesting outputs can be drawn. In such configurations an analytical evaluation is possible and appears to be a good tool to interpret the results given by the codes. This allows identifying the parameters or material properties with the main impact on the final heat flux applied to the vessel wall:

- In adiabatic case, only the correlations used in the oxide pool have an impact on the heat flux. This discrepancy may be limited when using the "best estimate" correlations, i.e. the correlations which have been validated for the highest Rayleigh numbers.
- In the case with radiative heat loss, the temperatures evaluated for the layers have an impact on the heat flux applied to the vessel wall since the power dissipated by radiation is directly linked with the metal layer temperature. In this case, the impact of the uncertainties on the material properties have been highlighted:
    - The metal layer has the main impact, with first its viscosity, then its melting temperature and its emissivity. A large uncertainty on the value of the thermal expansion coefficient was also identified.
    - The oxide layer impacts with its conductivity and its thermal expansion coefficient but it remains second order compared to the metal properties.

4.2Transient configuration

Transient configurations were also studied, considering a progressive incorporation of steel due to the melting of the internal structures in the vessel and evaluating the vessel wall ablation till reaching a stabilized situation. The initial corium composition at core relocation considered in this test is the same as the one defined for the first calculations (cf. Table 1), except for the steel mass which is reduced in order to simulate the progressive melting of the different metallic structures. For the sake of comparison between codes and to focus on the corium pool behaviour, the kinetics of molten steel addition in the corium pool are prescribed (6kg/s from 2h30 (9,000s) to about 4h (14,000s)[6]) instead of letting the codes simulate the progressive melting of the structures itself. The radiative boundary condition defined in case n°2 is considered. It should be noted that in ATHLET-CD code, it was not possible to impose this

[6] The rate of 6kg/s is evaluated considering a power of 1.8MW due to radiative heat transfers from the top surface of the corium pool and an enthalpy of fusion of steel equal to 300kJ/kg. The order of magnitude of the time needed to heat these metallic structures up to the melting point (2h30) is evaluated considering a power of 1.8MW coming from the corium pool, an initial temperature of 600K and an average heat capacity of 540J/K/kg over the range [600K-1600K].

arrival of molten steel during the stand alone lower plenum simulation. Thus, the results are considered only for the first phase (up to 9,000s).
In Figure 8, the heat flux profile at the outer surface of the vessel wall, at the time the maximum value is reached during the transient is presented. For all codes, the maximum value is reached before the beginning of the molten steel addition at 9,000s. It is evaluated in front of the top metal layer whose thickness is reduced to about 50cm (including molten steel from vessel ablation, against 90cm in the previous steady states). Values are in the range 0.55-0.85MW/m².

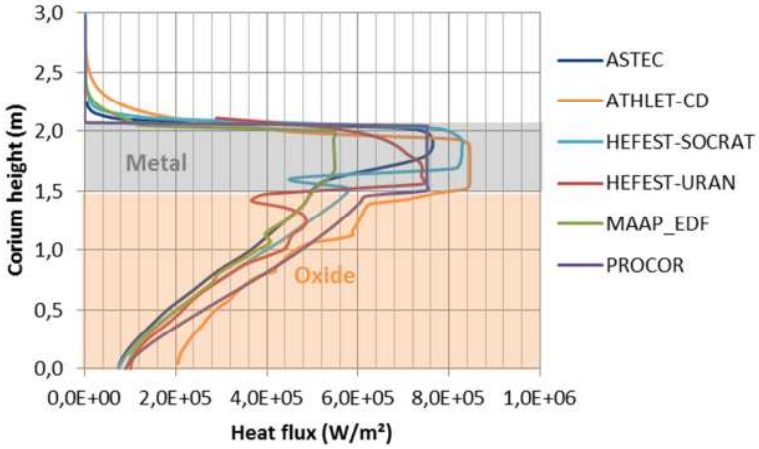

Figure 8 Heat flux profile at the outer surface of the vessel at the time the maximum value is reached (case n°3)

Based on the understanding of the differences between the codes presented in the previous part, it appears that the lowest value is associated to the strong radiative heat flux evaluated in this case in MAAP_EDF code, and mainly linked to the values of the metal layer properties. This is confirmed in Figure 9 a) where the power dispersion is presented for all simulations. In MAAP_EDF up to 25% is dissipated thanks to the radiative heat transfers at 9,000s.
During the transient, the two phases are clearly visible in all simulations: at the beginning, the residual power is only partly dissipated through the vessel and the rest is used to heat up the pool and the vessel wall and progressively melt it. This leads to the increase of the power fraction dissipated by external cooling. A quasi steady state is reached before the beginning of the molten steel injection at the top of the pool. This steel is at the liquidus temperature and needs to be heated up to reach again a stable configuration in which the residual power is entirely extracted by the external cooling and by the radiative heat transfers.

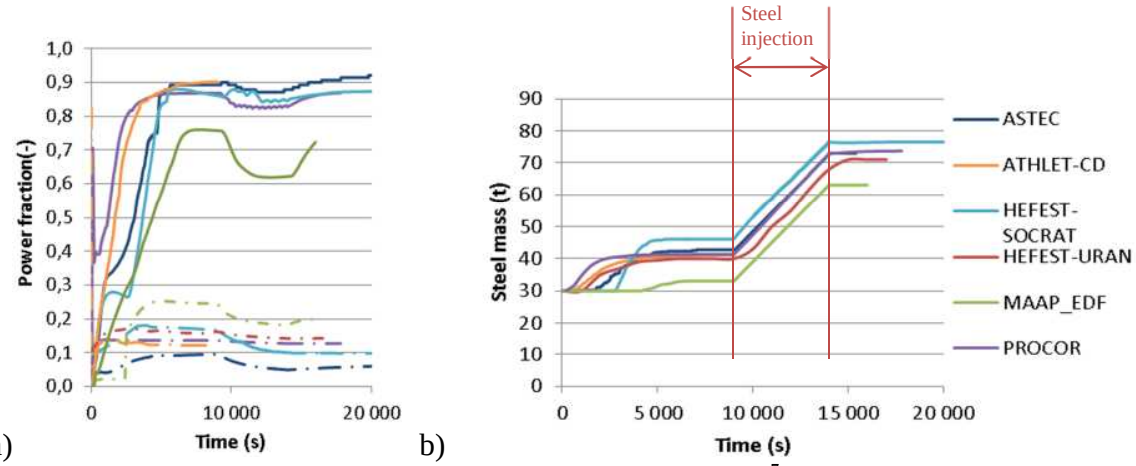

Figure 9 a) Fraction of residual power dissipated by the external cooling[7] (full lines) and by the radiation at the top of the pool (dashed lines); b) Evolution of the mass of molten steel incorporated in the metallic layer (case n°3)

[7] Data not available for HEFEST-URAN simulation

In Figure 9 b), the evolution of the mass of steel added to the metal layer is presented. It appears that the melting of the vessel wall happens mainly at the beginning of the transient and leads to add about 10-15t of steel into the metal layer, except for the MAAP_EDF simulation in which the molten steel added in the top layer from the vessel ablation is limited to 3t. This is of course directly linked with the evaluation of a smaller heat flux applied to the vessel wall in front of the metal layer due to larger dissipation by radiation. In addition, in ASTEC and MAAP_EDF simulations, the molten steel from the vessel wall in front of the oxide pool is kept in this layer and not considered in the evaluation presented in Figure 9 b), since thermochemical models are disabled in this case. It represents an additional mass of 7t in ASTEC and 4.7t in MAAP.
The profiles of ablated vessel wall obtained at steady state are summarized in Figure 10 a). The minimum thickness is reached in front of the bottom of the metallic layer, where the maximum heat flux was reached during the transient. The value is in the range 3-7cm. The dispersion of $\pm 21\%$ in the maximum heat flux evaluated at the outer surface of the vessel wall leads to a dispersion of $\pm 40\%$ in the evaluation of the minimum vessel thickness. If the case of MAAP_EDF calculation is not considered, the variability of the minimum thickness is reduced to $\pm 25\%$ corresponding to ± 1cm. It is worth noting that, in HEFEST-URAN simulation, the modelling of the oxide crust limits the heat flux and hence, the vessel ablation at its location.
Compared to the equivalent steady state case n°2, the maximum heat flux is multiplied by a factor 1.4-1.7. The steady-state profiles of heat flux at the outer surface of the vessel wall obtained are summarized in Figure 10 b). Except for the PROCOR result, these profiles significantly differ from the ones calculated in the case n°2, showing the importance of simulating the transient scenario to catch the evolution of the vessel ablation which has a direct impact on the heat flux distribution at the end. Indeed, it is shown that at the location of the minimum vessel thickness (between elevations 1.5-2m), the heat flux remains higher, even if the thickness of the top metal layer has increased (up to 2.5m). This effect is not visible in the PROCOR simulation due to the simplified meshing of the vessel wall which is used (1D axial meshing).
Reason for higher ablation of the vessel wall in the oxide part in HEFEST-SOCRAT simulation may be associated to the conductivity considered for the vessel wall, since the heat fluxes obtained at this location are comparable with other simulations and ablation in front of the metal layer is also more significant with respect to the level of maximum heat flux evaluated (cf. Figure 8).

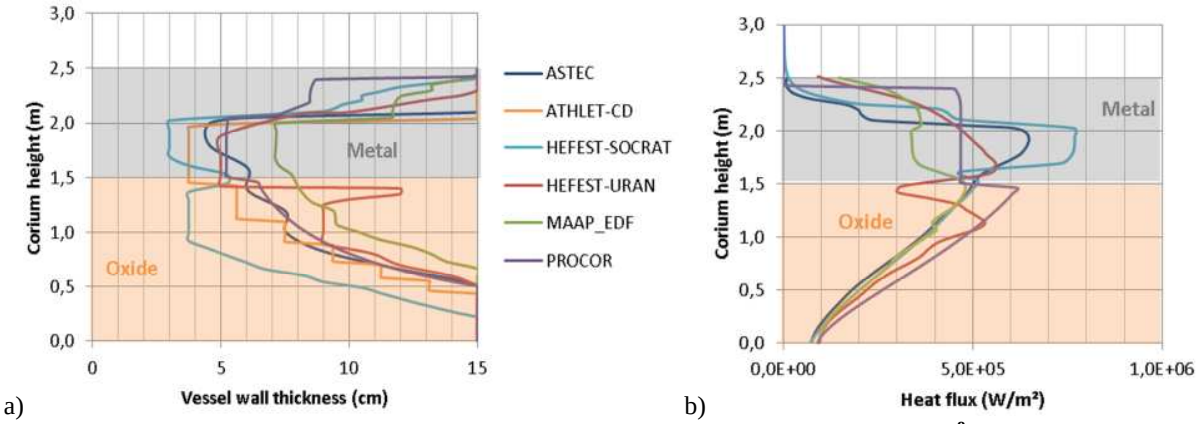

a) b)

Figure 10 Profiles of ablated vessel wall (a) and heat flux (b) at steady state[8] (case n°3)

The analysis of this case n°3, allows a clear identification of the impact on the minimum vessel thickness of the kinetics of molten steel addition. Depending on the time necessary to heat up and melt the metallic structures and in particular for structures located above the molten pool, a transient maximum heat flux may be reached for a time sufficiently long to melt the vessel wall more than in the "virtual" steady-state case. This ablated profile of the vessel has then an impact on the heat flux profiles obtained in steady state: the reduction of the thermal resistance at the location of the minimum vessel thickness obtained in transient configuration, allows an increase of the heat flux at the external vessel surface at this location at steady state.

[8] Note that, for ATHLET-CD simulation, the ablated profile is obtained at the end of the first phase without considering the injection of molten steel. Heat flux profile at steady state is not compared.

4.3Influence of thermochemical phenomena

In this last test, the thermochemical phenomena occurring in the corium pool are taken into account when associated modelling is available in the codes (ATHLET-CD did not take part to this case). Indeed, in the cases before, the non oxidized Zirconium was considered initially mixed with the molten steel. In reality, when the corium relocates from the core part it is composed of UO_2 and partially oxidized Zirconium (ZrO_2, Zr). Then, when mixed with molten steel, the metal and the oxide phases become non miscible but the metal phase becomes enriched in metallic Uranium. Thus, compared to the previous simple assumption, the composition of the metal phase at thermochemical equilibrium differs, with less Zr and more U. In addition, due to this interaction, fission products which have affinity with the metal phase migrate in this layer leading to partition of the residual power between the metal and oxide layers.
Results of heat flux profiles when the maximum is reached at the outer surface of the vessel are presented in Figure 11. A strong variation of the maximum heat flux is observed in the PROCOR simulation, where the maximum heat flux is reached at the top of the metal layer before injection of molten steel. This high heat flux (up to 5MW/m²) is due to a strong focusing effect occurring in a thin top layer of steel, once the molten steel has interacted with the oxide pool and been transferred below the oxide crust, as shown in Figure 13, with the progressive reduction of top metal layer thickness before molten steel injection and after the stop of injection. In other codes, such assumption regarding the metal relocation below the oxide crust is not made and the oxide crust is supposed to remain at the interface between the oxide and the metal layer, even during chemical interaction and transfer of Zirconium and Uranium in the metal layer. Despite the decrease of the oxide pool mass/height during this interaction, no oxide crust is considered in the front of the metal layer, assuming that it will lose its integrity. In PROCOR code, this lateral oxide crust in front of the metal layer after its interaction with this oxide leads to significantly decrease the heat flux at this location (below 0.2MW/m²).
Not considering the case of PROCOR code, the maximum heat fluxes obtained (0.64-1.1MW/m²) show an increase by a factor 1.2-1.3 compared to the test n°3 and thus 1.6-2.4 compared to steady-state simulation (test n°2).

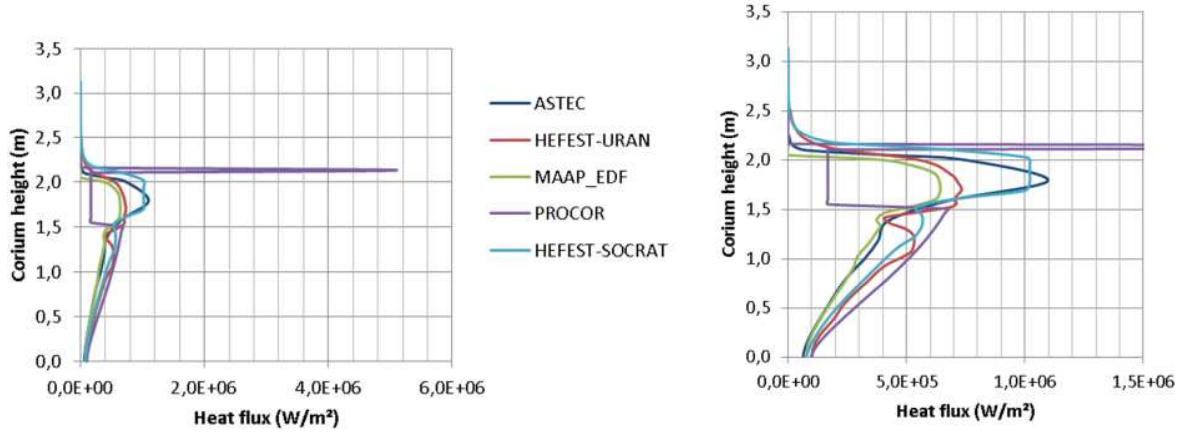

Figure 11 Profiles of heat flux along the outer vessel wall when maximum is reached (left) and zoom on low values (right) (case n°4)

In Figure 12, the profiles of ablated vessel wall at steady state show a reduction of the minimum vessel thickness compared to the previous case (n°3). This reduction due to the consideration of thermochemical effects is consistent for all codes and equal to about 1cm, except for PROCOR code, in which the minimum thickness is reduced of 4cm. The composition of the metal layer is modified due to the thermochemical interaction as presented in Figure 13, with incorporation of about 8-8.5t of metallic Uranium and reduction of the mass of Zirconium (3-4t) compared to the previous case n°3 (7.5t). This interaction with the oxide pool is very fast in ASTEC, HEFEST-SOCRAT and HEFEST-URAN codes and takes about 5,000s in MAAP_EDF and PROCOR codes. It is also associated to a transfer of fission products in the metallic phase leading to have a fraction of the residual power (15-20%) in the metal as illustrated in Figure 12. Finally, it could be noticed that the thermochemical equilibrium model used in ASTEC, MAAP_EDF and PROCOR (from Salay and Fichot, 2005), allows miscibility of a small part of UO_2 and ZrO_2 in the metallic phase (2t).

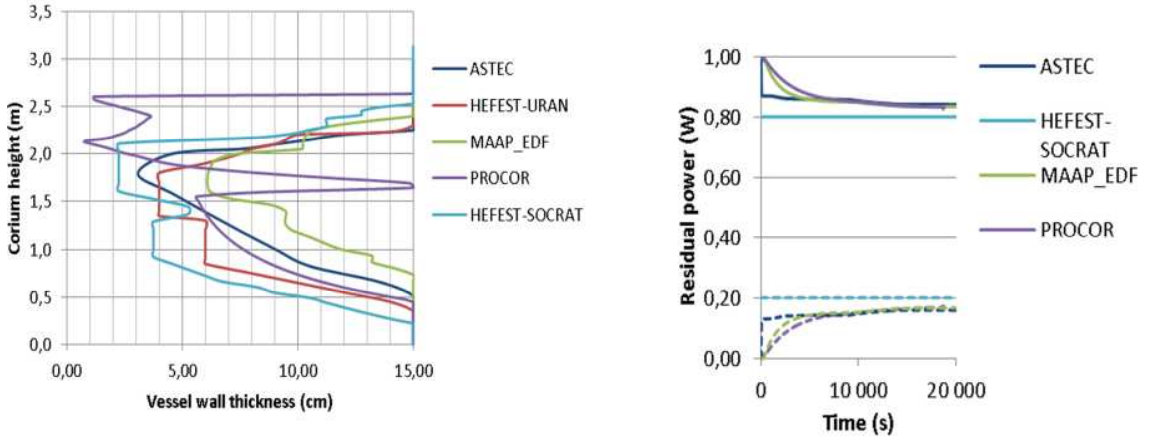

Figure 12 Ablated vessel wall at steady state (left) and residual power distribution between oxide (full lines) and metal (dashed lines) phases[9] (right) (case n°4)

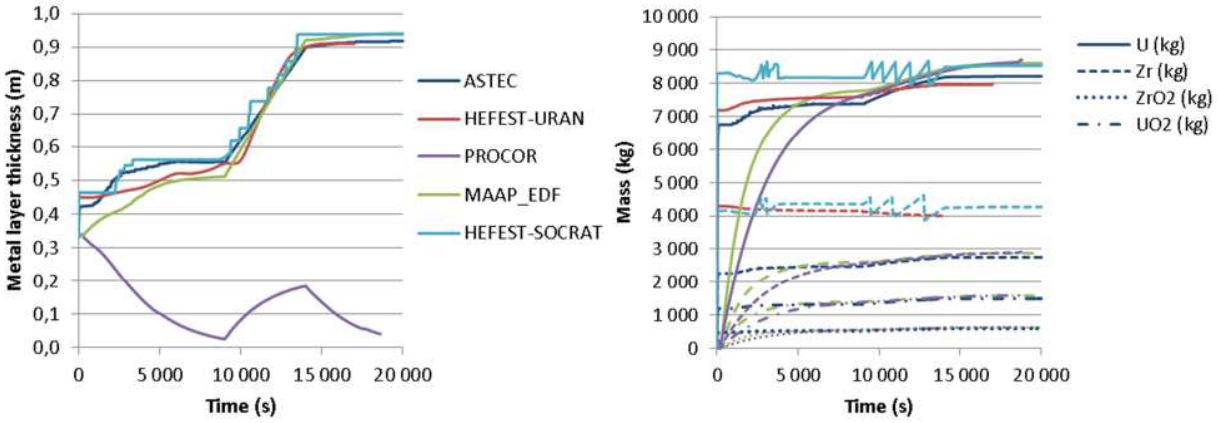

Figure 13 Evolution of the thickness (left) and of the composition[10] (right) of the top metal layer (case n°4)

4.4 Sensitivity analysis

A sensitivity analysis based on the last transient configuration (case n°4), which is the more complete and involved all the relevant phenomena was also performed. The idea was to cover the variation of the main parameters identified as leading to the main differences in the steady-state configurations (cf. § 4.1), in the range between lower and upper values implemented by default in the different codes used:

- Liquidus temperature of the metallic layer ([1600K-1778K], the solidus being defined 50K below);
- Dynamic viscosity of the metallic layer [4.07×10^{-3} – 2.24×10^{-2} Pa.s];
- Thermal expansion coefficient of the metal layer [2.9×10^{-5}-1.17×10^{-4} K^{-1}];
- Emissivity of the top metal layer [0.2-0.4].

A set of 200 calculations was defined for this sensitivity study. ASTEC, MAAP[11] and PROCOR codes participated in this study. In the case of PROCOR, the modelling of the crust being the main contributor to the minimum vessel

[9] It is constant and usually taken as 15% in the metal / 85% in the oxide in HEFEST-URAN code, in accordance with data from Ozrin et al. (2013)
[10] For PROCOR, it is the composition of the metal layer after interaction below the oxide crust. The top layer remains only composed by steel.
[11] Coupled with OpentTUNS (Baudin et al. 2015)

thickness obtained, the sensitivity study was performed considering the calculation n°3 (without effects of thermochemistry).

The range of variation of the minimum thickness of the vessel wall obtained is presented in Figure 14 and is in accordance with the range of results obtained by the different codes. This analysis illustrates the non negligible impact of the metal layer properties and of the associated uncertainties. As expected, without considering the thermochemical effects (PROCOR evaluations) the values for the minimum thickness are higher.

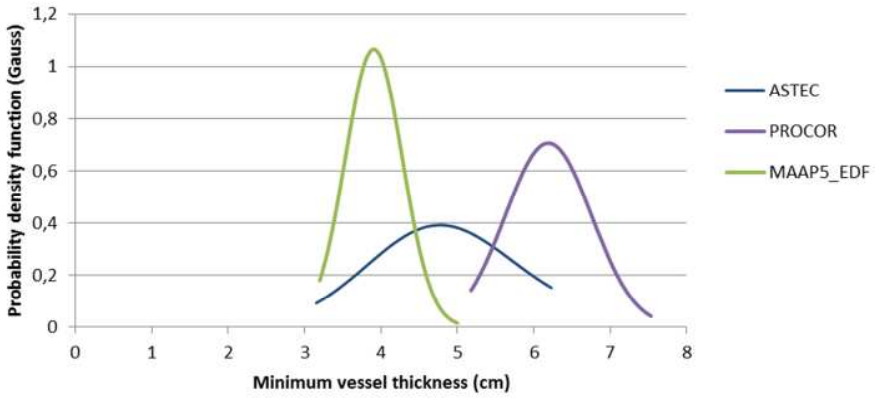

Figure 14 Probability density function obtained for the minimum vessel thickness in case n°4 for ASTEC, and MAAP and in case n°3 for PROCOR

Results of the standard regression coefficients obtained for the 4 parameters considered show that the melting temperature of the metal layer and its emissivity are the main parameters, which impact significantly the power dissipated by radiation in this test configuration. Then, the viscosity of the metallic layer and its thermal expansion coefficient also play a role, as previously identified in Figure 6.

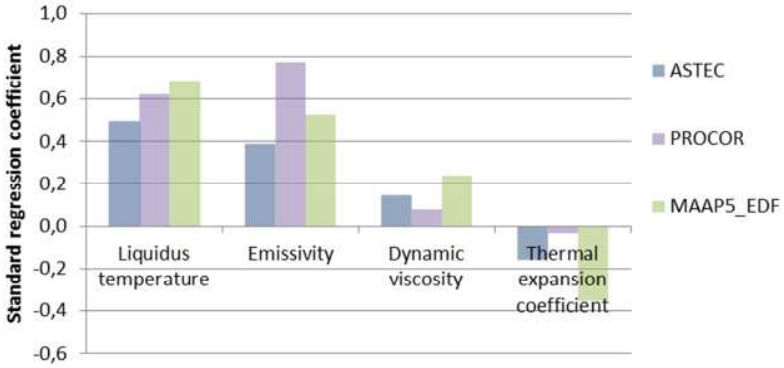

Figure 15 Standard regression coefficient obtained for the minimum vessel thickness in case n°4 for ASTEC and MAAP and in case n°3 for PROCOR

5. Conclusion

A benchmark exercise on IVR was performed between 6 different codes in order to compare the best estimate results of each code and get a deeper understanding of the differences between implemented models. The exercise was made by the code developers themselves to limit somehow the potential user-effect. This crosswalk study followed a step by step approach with a gradual increase of complexity. It must be noted that a detailed comparison for lower head vessel modelling was already performed between MAAP_EDF and PROCOR codes (Bakouta et al., 2015) but it is the first exercise of this kind involving 6 different codes, either integral or dedicated to the lower head.

It was first checked that, when considering steady state configurations, the variability of the results for the evaluation of the maximum heat flux along the outer surface of vessel wall remains limited ($\pm 20\%$). It was highlighted that this dispersion is mainly due to the uncertainties in the metal layer dynamic viscosity, thermal

expansion coefficient, emissivity and melting temperature. It may be noted that this dispersion is even lower than the one evaluated for the AP1000 case by (Esmaili et al. 2004). This can be explained by the smaller number of uncertain parameters and of layer configurations considered.
Then, the importance of performing transient evaluation of IVR was illustrated by taking into account the progressive addition of steel in the corium due to melting of the vessel and of the upper structures. Because of the presence, at the beginning of the transient, of a thin metal layer, the results of all codes indicate a possible increase of the maximum heat flux evaluated at the outer surface of the vessel. In such transient simulations, a large variability of the results for the minimum vessel thickness was evaluated (about $\pm 80\%$), with a variation from less than 1cm to 6cm. The differences between models leading to the most significant discrepancies in minimum vessel thickness evaluation have been identified, and the modelling of the oxide crust appears to play a major role. Depending on modelling assumption, this oxide crust is assumed to be present around the metal layer (due to the chemical equilibrium with the oxide) or not (non equilibrium situations). The chemical stability of the crust and its impact on the kinetics of stratification were recently studied in the CORDEB experiments (Almjashev et al., 2018). It clearly indicates that the crust is stable for only a limited period of time and that the oxide/metal system may evolve out of equilibrium for some time. But further studies are needed to validate the modelling implemented in the codes. In particular, it is of primary importance to evaluate the stability of the lateral oxide crust in front of the metal layer after interaction and estimate the time during which it can be considered as a thermal resistance.
Looking at a simpler situation where the thermochemical interactions between the corium pool and the molten steel are neglected, this dispersion in minimum vessel thickness evaluation is reduced to $\pm 40\%$ corresponding to $\pm 2cm$. A dedicated sensitivity analysis has shown the main contributors to that dispersion are the uncertainties on physical properties of the metal layer. The impact of other parameters and specificities of models implementation in the codes appears to be less significant.
In the current context of construction of Gen III plants throughout the world, many of them with IVR strategy, there is a need for a strong assessment of the codes used for safety evaluation. The set of situations considered and the results presented might be used as a reference for other codes, to demonstrate their ability to simulate IVR in steady-state and transient situations, taking into account the latest knowledge on thermochemistry and oxide/metal stratification.
It should be mentioned that the configurations presented in this paper do not involve the simulation of the formation of a heavy metal layer followed by the transient stratification inversion. This more complex situation is expected to be more challenging for the codes and will be considered in the final step of this benchmark activity in the scope of the IVMR project.

6. Acknowledgments

The authors wish to acknowledge funding and support provided by the European Project H2020 IVMR No. 662157.

7. References

Almjashev V.I., Granovsky V.S., Khabensky V.B., Kotova S.Yu., Krushinov E.V., Sulatsky A.A., Vitol S.A., Gusarov V.V., Fichot F., Michel B., Piluso P., Le Tellier R., Fischer M., Le Guennic C., Bakouta N., Experimental study of transient phenomena in the three-liquid oxidic-metallic corium pool, *Nuclear Engineering and Design*, 332, pp. 31-37, 2018

Asfia S.J., Dhir V.K., An experimental study of natural convection in a volumetrically heated spherical pool bounded on top with a rigid wall, *Nuclear Engineering and Design* 163, p 333-348, 1996

Bakouta N., Le Tellier R. & Saas L., Assessment of advanced corium-in-lower-head models in MAAP and PROCOR codes, proceedings of the *7th European Review Meeting on Severe Accident Research ERMSAR*, 2015.

Bonnet J.M., Seiler J.M., Thermal hydraulic phenomena in corium pool: the BALI experiment, proceedings of *ICONE7 Conference*, Tokyo (Japan), 1999.

Carénini L., Fichot F., The Impact of Transient Behavior of Corium in the Lower Head of a Reactor Vessel for In-Vessel Melt Retention Strategies, proceedings of *ICONE24 Conference*, Charlotte (USA), 2016.

Chawla T.C. and Chan S.H., Heat transfer from vertical/inclined boundaries of heat generating boiling pools, *Journal of Heat Transfer*, Vol.104, pp. 465–473 (1982)

Bakouta N., Torkhani M., La Belguet A., In-vessel corium modelling in the MAAP_EDF code, proceedings of the *8th ERMSAR conference* (European Review Meeting on Severe Accident Research) Warsaw, Poland, 15-18 Mai 2017.

Baudin M., Dutfoy A., Iooss B., Popelin AL. OpenTURNS: An Industrial Software for Uncertainty Quantification in Simulation. In: Ghanem R., Higdon D., Owhadi H. (eds) Handbook of Uncertainty Quantification. Springer, Cham, 2015. https://rd.springer.com/referenceworkentry/10.1007/978-3-319-11259-6_64-1

Churchill S. W., Chu H. H., Correlating equations for laminar and turbulent free convection from a vertical plate, *Int. J. Heat Mass Transfer*, Vol. 18, pp. 1323-1329, 1975.

Duspiva J., Progress in Simulation of IVR Strategy for VVER-1000/320 Reactor with MELCOR code, proceedings of *17th NURETH Conference*, Xi'an (China), September 3-8, 2017.

Esmaili H., Khatib-Rhabar M., "Analysis of in-vessel retention and ex-vessel fuel coolant interaction for AP-1000", NUREG/CR-6849, ERI/NRC 04-201, 2004.

Fichot F., Carénini L., Sangiorgi M., Hermsmeyer S., Miassoedov A., Bechta S., Zdarek J., Guenadou D., Some considerations to improve the methodology to assess In-Vessel Retention strategy for high-power reactors, *Annals of Nuclear Energy*, Vol. 119, pp. 26-45, 2018.

Filippov A.S., Drobyshevsky N.I., Kisselev A.E., Strizhov V.F., Fokin A.L. SOCRAT/HEFEST code: models of VVER core melt interaction with reactor structures under severe accident conditions // *Bull. Russ. Acad. Sci.*, Energetics, 3, P.4-24, 2010 (in Russian).

Filippov A.S., Drobyshevsky N.I., Kamenskay D.D., Kisselev A.E., Moiseenko E.V. End-to-end technology of modeling a melt-structure interaction during IVMR in VVER with HEFEST-URAN toolkit. Proc. 22nd *Int. Conf. Nuclear Engineering, ICONE22*, Prague (Czech republic), July 7-11, 2014.

Gencheva R., Stefanova A., Groudev P., Chatterjee B., Mukhopadhyay D., Study of in-vessel melt retention for VVER-1000/v320 reactor, *Nuclear Engineering and Design*, 298, pp. 208-217, 2016.

Henry R.E., Fauske H.K., "External cooling of a reactor vessel under severe accident conditions", *Nuclear Engineering and Design*, Vol.139, pp. 31-43, 1993.

Jahn M., Reinke H.H., "Free convection heat transfer with internal energies sources: calculation and measurements", proceedings of the *5th Int. Heat Transfer Conference*, Tokyo (Japan), 1974.

Kelkar K.M., Khankari K.K., Patankar S.V., Computational modelling of turbulent natural convection in flows simulating reactor core melt, *Final Rep, Sandia National Laboratories*, Albuquerque, NM, December 1993

Knudson D.L., Rempe, J.L., Condie K.G., Suh K.Y., Cheung F.-B., Kim S.-B., " Late-phase melt conditions affecting the potential for in-vessel retention in high power reactors", *Nuclear Engineering and Design*, Vol. 230, 2004.

Kymälainen O., Tuomisto H. and Theofanous T.G., In-vessel retention of corium at the Loviisa plant, *Nuclear Engineering and Design*, 169, 1997.

Le Tellier R., Saas L., Bajard S., Transient stratification modelling of a corium pool in a LWR vessel lower head, *Nuclear Engineering and Design* 287, pp. 68-77, 2015.

Pandazis P., Weber S., Investigation of a severe accident late phase scenario in a PWR with ATHLET-CD, proceedings of the *27th Nuclear Energy for New Europe Conference*, Portoroz (Slovenia), 2018.

Ozrin V.D., Tarasov V.I., Filippov A.S., Moiseenko E.V., Tarasov O.V.. Distribution of fission product residual decay heat in stratified core melt of LWR and its influence on sidewall heat flux. // *Nucl. Eng. Des.* 107-115, Vol. 261, 2013.

Rempe J.L., Knudson D. L., Allison C. M., Thinnes G.L., Atwood C.L., Cebull M.J., Potential for AP600 In-Vessel Retention through Ex-Vessel Flooding, INEEL/EXT-97-00779, December 1997.

Rempe J.L., Knudson D.L., Condie K.G., Suh K.Y., Cheung F.-B., Kim S.-B., Corium retention for high power reactors by an in-vessel core catcher in combination with External Reactor Vessel Cooling, *Nuclear Engineering and Design*, Vol. 230, 2004.

Salay M. and Fichot F., Modeling of metal-oxide corium stratification in the lower plenum of a reactor vessel, Proceedings of *NURETH-11 Conference*, Avignon (France), 2005.

Theofanous T.G., Liu C., Addition S., Angelini S., Kymälainen O. and Salmassi T., In-vessel coolability and retention of core melt, *Nuclear Engineering and Design*, Vol. 169, 1997.

Tsurikov D., MASCA2 Project: Major Activities and Results, Proceedings of *MASCA2 Seminar*, Cadarache (France), October 11-12, 2007.

Tuomisto H., Theofanous T.G., A consistent approach to severe accident management, *Nuclear Engineering and Design*, Vol. 148, 1994.

Whang S., Park H.S., Moriyama K., Lim K., Cho Y.J., Kim M.H., Uncertainty analysis of in-vessel retention in a high power reactor during severe accident, *Nuclear Engineering and Design*, Vol. 319, 2017.

Xing J., Song D., Wu Y., HPR1000: Advanced Pressurized Water Reactor with Active and Passive Safety, *Engineering*, Vol. 2, pp. 79-87, 2016.

Zdarek J., Krhounek L., Batek D., Zvonarev Yu., Volchek A., Kobzar V., Budaev M., Assessment of In-Vessel Melt Retention possibility for VVER-1000/320, proceedings of *6th European Review Meeting on Severe Accident Research (ERMSAR-2013)*, Avignon (France), October 2-4, 2013.

Appendix A – Analytical evaluation of steady state configurations (tests n°1 and 2)

Nomenclature

Latin letters

C_p	Heat capacity [J/K/kg]
D	Diffusion coefficient [m²/s]
g	Standard gravity [m/s²]
H	Layer height [m]
k	Thermal conductivity [W/m/K]
P_{res}	Residual power [W]
$\dot{Q}$	Volumetric power [W/m^3]
R	Vessel radius [m]
S	Surface [m²]
T_{liq}	Liquidus temperature [K]
T_{pool}	Bulk temperature of the layer [K]

Grec letters

α	Thermal diffusivity [m²/s] $\left(\alpha = k/\rho.C_p\right)$
β	Thermal expansion coefficient [K^{-1}]
ε	emissivity [-]
φ	Heat flux [W/m²]
ν	Kinematic viscosity [m²/s]
ρ	Density [kg/m^3]
μ	Dynamic viscosity [Pa.s]

Steady-state configurations n°1 and 2 defined for the benchmark exercise (cf. Figure 1) may be evaluated in an analytical way. The order of magnitude of the heat fluxes and the layers temperatures are estimated in the following parts. The values of the physical properties used for this simple evaluation are the ones presented in the table below.

Table 4 – Material properties corresponding to the benchmarking case (from Esmali and Khatib-Rahbar, 2004)

	Parameter	Value
Oxide pool	Density	8191 kg/m^3
	Thermal conductivity	5.3 W/m/K
	Dynamic viscosity	4.67x10^{-3} Pa.s
	Specific heat capacity	533 J/kg/K
	Thermal expansion coefficient	1.05x10^{-4} K^{-1}
	Melting temperature	2950 K
Metallic pool	Density	6899 kg/m^3
	Thermal conductivity	25 W/m/K
	Dynamic viscosity	4.07x10^{-3} Pa.s
	Specific heat capacity	789.5 J/kg/K
	Thermal expansion coefficient	1.11x10^{-4} K^{-1}
	Melting temperature	1600 K

I. Determination of the temperature of the oxide pool

It is assumed here that all the residual power is produced in the oxide pool. The governing parameter is the internal Rayleigh number:

$$Ra_{ox} = \frac{g\beta_{ox}\dot{Q}_{ox}H^5}{\alpha_{ox}k_{ox}\upsilon_{ox}}$$

In the present case, the oxide pool has a height $H{\sim}1.5m$. The residual power in the oxide pool of $P_{res} = 14MW$ corresponds to a volumetric power of $\dot{Q}_{ox}{\sim}1.3MW/m^3$. This gives $Ra_{ox}{\sim}3.10^{15}$.
There is a partition of that power and one part is transferred to the vessel wall ($\varphi_{dn}S_{dn}$) and the complementary part is transferred to the top metal layer ($\varphi_{up}S_{up}$).

$$\varphi_{dn}S_{dn} + \varphi_{up}S_{up} = P_{res}$$

Heat fluxes are evaluated thanks to experimental correlations, assuming that the oxide pool is surrounded by a crust which imposes a uniform boundary condition at the liquidus temperature of the oxide mixture: T_{liq}^{ox}. With this assumption, both heat fluxes are expressed as a function of the temperature difference ($T_{pool}^{ox} - T_{liq}^{ox}$).

$$\varphi_{dn} = \frac{k_{ox}}{H}Nu_{dn}(T_{pool}^{ox} - T_{liq}^{ox});\ \varphi_{up} = \frac{k_{ox}}{H}Nu_{up}(T_{pool}^{ox} - T_{liq}^{ox})$$

From that, we directly get the temperature of the oxide pool:

$$T_{pool}^{ox} = T_{liq}^{ox} + P_{res}\frac{H}{k_{ox}}\left(Nu_{dn}S_{dn} + Nu_{up}S_{up}\right)^{-1}$$

If we choose COPO/BALI correlations (Bonnet and Seiler, 1999), we get:

$$Nu_{dn} = 0.131{Ra_{ox}}^{0.25}\left(\frac{H}{R}\right)^{0.19};\ Nu_{up} = 0.381{Ra_{ox}}^{0.234}$$

And $T_{pool}^{ox} = T_{liq}^{ox} + 110$, where the liquidus temperature of the oxide may vary according to the code or the user's choice and is considered in this benchmark at $T_{liq}^{ox}{\sim}2950K$.

II. Determination of the partition of power in the oxide between top and bottom

One important point is that, with the assumptions chosen, the partition of residual power between bottom and top is independent of the boundary conditions and depends only on the internal Rayleigh number and on the shape of the vessel:

$$\frac{\varphi_{up}}{\varphi_{dn}} = \frac{Nu_{up}}{Nu_{dn}} = \frac{0.131}{0.381}{Ra_{ox}}^{(0.234-0.25)} \text{ and } \frac{\varphi_{up}S_{up}}{\varphi_{dn}S_{dn}+\varphi_{up}S_{up}} = \frac{Nu_{up}S_{up}}{Nu_{dn}S_{dn}+Nu_{up}S_{up}}{\sim}0.52$$

Therefore, we see that close to 50% of the residual power is transferred to the top metal layer, independently of the boundary conditions. With the surfaces considered in this benchmark, the bottom and top heat fluxes are:

$$\varphi_{dn} = 0.36MW/m^2;\ \varphi_{up} = 0.62MW/m^2$$

III. Determination of the maximum heat flux in the oxide

Correlations derived from experimental data provide the heat flux profile along the vessel wall: $\frac{Nu(\theta)}{Nu_{dn}} = f(\theta)$.

The maximum value is found at the top. Using the distribution function proposed in Theofanous et al. (1996) for a hemispherical vessel leads to a "peaking factor" of 1.8 and, therefore:

$${\varphi_{dn}}^{max} = 0.64MW/m^2$$

IV. Determination of the heat flux along the top metal layer

For the metal layer, natural convection is driven by the contact with the hot oxide pool and the cooling along the side wall and also, possibly, at the top of the metal layer (radiative heat transfer). The standard Rayleigh number is used:

$$Ra_{met} = \frac{g\beta_{met}\left(T_{pool}^{met} - T_{liq}^{wall}\right){H_{met}}^3}{\alpha_{met}\upsilon_{met}}$$

The expression of the heat flux along the side wall is:

$$\varphi_{met} = \frac{k_{met}}{H_{met}} Nu_{met}\left(T_{pool}^{met} - T_{liq}^{wall}\right)$$

Where, using the Chawla-Chan correlation in turbulent regime (Chawla and Chan, 1982), we have:

$$\varphi_{met} = 0.076 k_{met}\left(\frac{g\beta_{met}}{\alpha_{met}\upsilon_{met}}\right)^{1/3}\left(T_{pool}^{met} - T_{liq}^{wall}\right)^{4/3}$$

If, we assume that there is no heat loss from the top (conservative assumption neglecting radiative heat transfer with upper structures), the conservation of energy gives: $\varphi_{up} S_{up} = \varphi_{met} S_{met}$
We recall that, because of the partition of energy found previously, this is equivalent, in the present case, to the relation: $\varphi_{met} S_{met} = 0.52 P_{res}$
Therefore we obtain, for the heat flux along the metal layer (for a height of metal layer estimated to 90cm):

$$\varphi_{met} = 0.64\ MW/m^2$$

If we assume a radiative heat flux with the upper structures: $\varphi_{met} S_{met} + \varphi_{radi} S_{up} = 0.52 P_{res}$
With $\varphi_{radi} = \varepsilon\sigma\left({T_{up}}^4 - {T_{structures}}^4\right)$

Using the Globe-Dropkin correlation (Globe and Dropkin, 1959) for the upwards heat transfers, allows evaluating the heat flux repartition, considering $T_{structures} = 950K$ and $\varepsilon = 0.38$:

$$\varphi_{met} = 0.5\ MW/m^2;\ \varphi_{radi} = 0.15\ MW/m^2$$

V. Determination of the temperature of the metal pool

The temperature of the metal pool, in the case $\varphi_{met} = 0.5\ MW/m^2$, is obtained by:

$$T_{pool}^{met} = T_{liq}^{wall} + \left(\frac{\varphi_{met}}{0.076 k_{met}}\right)^{3/4}\left(\frac{\alpha_{met}\upsilon_{met}}{g\beta_{met}}\right)^{1/4} \sim T_{liq}^{wall} + 82$$

where the melting temperature of the wall is evaluated in this benchmark at $T_{liq}^{wall} \sim 1600K$.

VI. References

Bonnet J.M., Seiler J.M., "Thermal hydraulic phenomena in corium pool: the BALI experiment", proceedings of *ICONE7 Conference*, Tokyo (Japan) (1999)

Chawla T.C. and Chan S.H., "Heat transfer from vertical/inclined boundaries of heat generating boiling pools", Journal of Heat Transfer, Vol.104, pp. 465–473 (1982)

Globe S. and Dropkin D., "Natural convection heat transfer liquids confined by two horizontal plates and heated from below", Journal of Heat Transfer, Vol.81, pp. 24–28 (1959)

Theofanous T.G., Liu C., Additon S., Angelini S., Kymäläinen O., Salmassi T., "In-Vessel Coolability and Retention of a Core Melt". DOE/ID-10460, October 1996